Structural Coupled Electromagnetic Sensing of Defects Diagnostic System

Gaige Ru[1], Bin Gao[1*], Dong Liu[1], Qiuping Ma[1], Haoran LI[1], Wai Lok Woo[2]

[1]*School of Automation Engineering, University of Electronic Science and Technology of China, China*

[2]*Department of Computer and Information Sciences, Northumbria University, England, UK.*

Corresponding author: bin_gao@uestc.edu.cn

***Abstract*—Magnetic flux leakage (MFL) detection methods are widely used to detect pipeline defects. However, it is limited by the detection orientation and magnetization. Besides, bulky excitation systems are incapable of adapting to the complex detection environments. This paper proposes a new Electromagnetic Structured Coupling sensing of merging Alternating Current Field Measurement (ACFM) and MFL within a multi-parameter system for different types of pipeline defects detection. In particular, a novel electromagnetic coupling sensor structure is proposed which enables simultaneous interaction between the excitation modes of Yoke and coil. Magnetic Yoke is integrated to magnetizing the axial pipeline to detect the circumferential surface and subsurface defects while the coil excites the circumferential uniform alternating current field and recognizes the axial defect. The novel structured sensing is highly sensitivity to the detection of both surface and subsurface defects. Simulation and experiments on defects in several samples have been conducted to validate the reliability and efficiency of the proposed system.**

***Index Terms*—Pipeline defects, Magnetic Flux Leakage (MFL), Alternating Current Field Measurement (ACFM), multiphysics sensing.**

I. INTRODUCTION

The integrity assessment of pipelines has commanded significant attention in the oil and gas industry. However, in the service pipeline, structural damage, corrosion and geometric discontinuity in a harsh environment will affect the transportation performance and safety [1-2]. Fuel leakage in the pipeline may cause badly damage to the environment, resulting in explosion, fire and even injuries of pipeline network. In particular, the detection and quantification of different defects exist challenging of Nondestructive testing (NDT) in pipeline integrity diagnosis [3-5]. Among the NDT methods, magnetic flux leakage (MFL) testing is invariably used for pipeline crack detection. However, the limitations of MFL are insensitivity to crack parallel to the magnetization direction while subsurface defects are difficult to be distinguished due to the ambiguity of signal to noise ratio (SNR).

Besides MFL, other NDT techniques including Magnetic Particle Testing (MT), Penetration Testing (PT), Alternating Current Field Measurement (ACFM), Eddy Current Thermography (ECT), Ultrasonic Testing (UT), and Electromagnetic Acoustic Transducer (EMAT). MT is effective in detecting surface and near-surface flaws. However, due to the complex process, the detection efficiency is relatively low [6-7]. PT has the advantages of visually capturing the defects in complex structured specimens [8]. However, internal damages cannot be identified. ACFM can be used in quantitative evaluation of both length and depth of surface cracks while it has the capability of non-contact and rapid inspection [9-10]. ECT has been applied to structural health detection because of its high resolution, non-contact, controllability, and intuitiveness. Unfortunately, ECT system remains difficult to be applied for the subsurface defects of pipe [11-12]. UT has a high sensitivity for detecting deep crack because of the strong penetrability. However, it requires the coupling agent between the probe and the specimen [13]. The strength of EMAT can be used to detect inner flaws in non-contact with no coupling. However, the requirements of decent transducer energy ratio and SNR remain as limitations [14].

The single NDT method has limitation to detect multiple types of defects [15-17]. To mitigate these problems, the detectability and sensitivity can be significantly improved through the complementary strength of different sensing mechanisms. Many researches on hybrid testing have been carried out. Li *et al*. [18] proposed a structure of magnetic sensors array based on ACFM probe, which is adequate to detect defects with narrow string flaws of ferrimagnetic materials. Guo *et al*. [19] presented a novel physics perspective fusion of EMAT and eddy current testing (EC) which is capable of inspecting near-surface and internal defects of ferromagnetic and non-ferromagnetic material. Bang *et al.* [20] proposed a new guided wave testing technology for pipeline defect detection. It has high energy conversion ratio it is limited to small-diameter pipelines inspection. Li *et al*. [21] designed a novel multi-physics structured eddy current and thermography system for moving object inspection to ameliorate the influence of the surface emissivity and impurities. Zhang *et al*. [22] presented a three-phase currents probe, which can induce the rotated eddy current field in the material. For gathering high detection sensitivity with different orientations as well. Gotoh *et al*. [23] used an AC magnetic flux leakage to detect internal and external defects. At the same time, it can identify the number of defects to a certain extent. Toharaand *et al*. [24] proposed an excitation method which used square wave alternating magnetic based on DC bias, the internal and external defects of steel pipe can be detected. Liu *et al*. [25] illustrated a weak magnetic flux leakage inspection method to detect both inner and outer crack of pipeline. Gao *et al*. [26] suggested a sensing structure that combined MFL and ECT, which were used to evaluate and visualize artificial crack. Daryabor *et al*. [27] investigated the fusion of UT and ECT physical structure applied to detect the patches and bonding of aluminum plate. Besides, image fusion is used to improve the accuracy and reliability of detection results. Chen *et al.* [28] presented a high-sensitivity double-layer different planar probe to detect different types of surface defects under high lift-off, however, it fails to detect sub-surface defects. Sun *et al*. [29] presented a novel inspection method under axial magnetization, which is applied for detecting omni-directional defects. Xiao *et al.* [30] proposed a method to distinguish the inner and outer wall defects of pipeline by using the characteristics of pulse remote field eddy current signal due to it is fixed detection rather than mobile detection, the detection efficiency is limited. Pham *et al*.

[31] developed a novel device based on a planar hall magnetoresistance sensor which has high-sensitivity to shallow defects at inner and outer pipe wall. Tehranchi *et al*. [32] introduced a double-core giant magneto-impedance sensor to improve the quantification ability of surface defects. Deif S *et al.* [33] presented a Chipless radio frequency identification (RFID) technique for out-of-sight pipeline monitoring structure, which can detect and monitor the frequency characteristics of defects caused by water inflow under the pipeline coating, evaluating the pipeline corrosion. Piao *et al*. [34] developed a new high-speed probe that fusing MFL and EC method since it has a detection capability for near-surface flaws at high speed. In particular, circumferential defects, internal flaws, and complex excitation structure have always been difficult for pipeline detection.

This paper proposed a new rectangular-shaped ferrite magnetic excitation structure of coupling electromagnetic sensing to enhance the detectability. In this model, uniform eddy current field and primary magnetic flux field can be induced and gathered simultaneously in the region of interest (ROI) [35]. The magnetization of the specimen is increased, and the space size of the excitation structure is reduced. Compared with the traditional methods, the proposed model uses alternating excitation which shares the same sensing structure as well as integrating highly sensitive tunneling magneto-resistance (TMR) sensors for measuring magnetic signal as the receiver. This mode will not only maintain the sensitivity of surface defects detection, but also enable to detect deeper defects more effectively due to the MFL. It also increases strengthen the detection capability of different types of defects. A novel diagnostic system that physically integrates ACFM with MFL sensing mechanism is proposed. The detection capability of the proposed method has been demonstrated through simulations and real experiments.

The rest section of this paper is arranged as follows: Section 2 introduces the theoretical analysis of the proposed electromagnetic coupling methods. Section3 implements the 3-dimensional numerical simulation. Section 4 carried out experimental verification by the proposed sensing structure. Conclusion and the future works are presented in Section 5.

I. METHODOLOGY

A. Configuration of the proposed electromagnetic coupling sensor structure

A novel electromagnetic diagnostic system that physically integrates ACFM with Alternating Current Magnetic flux leakage (AC-MFL) sensing structure is shown in Fig. 1. Based on signal generator, a high-frequency sinusoidal signal is enlarged by a power amplifier. This drives the rectangular-shaped ferrite magnetic yoke to generate a strong axial magnetic flux field and induce a uniform circumferential alternating current field in the tested sample. The specific sensing structure is shown in Fig. 1. The copper coil is evenly wound in the middle of the rectangular-shaped yoke, and the TMR magnetic sensors are located in the middle of the yoke. These can be directly used to detect signals. The traditional U-type probe only uses magnetic yoke poles to excite sample whereas ignoring the importance of the excitation coil. A novel electromagnetic coupling sensor structure is proposed. It makes both excitation modes of pole and coil conduct an interaction simultaneously. This will improve the magnetization strength as well as reducing the geometry space of the excitation probe.

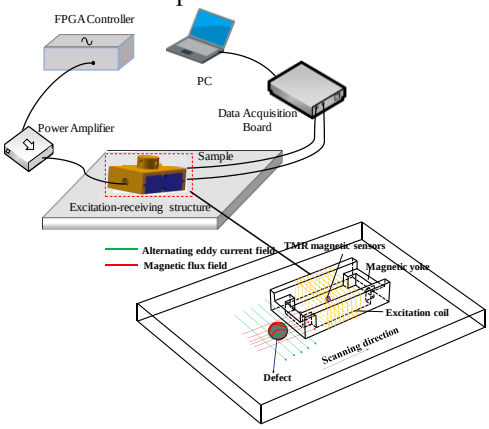

Fig. 1 Schematic diagram which shows the integration of ACFM with AC-MFL sensing structure.

According to Faraday's law, when a sinusoidal excitation is applied to the coil, a corresponding alternating magnetic field will be generated. When defects exist on the surface or subsurface of the ferromagnetic materials, the magnetic permeability and electrical conductivity of the crack will affect the intensity and distribution of the uniform alternating current field and the leakage magnetic field. By detecting the change of the magnetic intensity, it is used to horizontal and vertical defect detection. On the one hand, the alternating magnetization field is perpendicular to the surface defect, AC-MFL can be significantly effective for detecting surface discontinuity of the metal material. On the other hand, the alternating electromagnetic field is parallel to the defect direction, ACFM dominates detection role. Considering the skin effect, the ACFM technique is invalid for sub-surface defect since it increases the saturation magnetization depth. Thus, this improves the detectability of subsurface defects due to the large magnetoresistance at the defective region. Both detectability advantages of AC-MFL and ACFM technique can be handled. In particular, the magnetic lines will flow toward the upper part of the defect, and around the defect while leakage magnetic flux will appear on the surface of the sample. Finally, high sensitivity TMR magnetic sensor is used to capture leakage flux signal. The detection capability of both electric field and magnetic field can be fused based on the principle of physics coupling sensing mechanism.

B. Mathematical models of the proposed sensor structure

Through the analysis of excitation structure, the magnetic circuit generated by coil excitation is divided into four paths (Fig. 2). Firstly, the magnetic flux of Path2 and Path4 is required to traverse the specimen and then form a closed magnetic circuit. They are indicated by green and red dotted line, respectively. The average length of magnetic path within Path2 and Path 4 is l_2 and l_4, respectively. The difference can be drawn that the magnetic flux of Path 2 generated by the coil directly flows into the sample. The magnetic flux of Path 4 is generated by the yoke, and it enters the sample through the gap between the pole and the sample. Secondly, Path 1 and Path 3 conduct the magnetic flux leakage by coil flow into the air while these are represented as blue and purple dotted loop, respectively. The flux path of the blue dotted loop is denoted as l_1, and purple dotted loop is l_3.

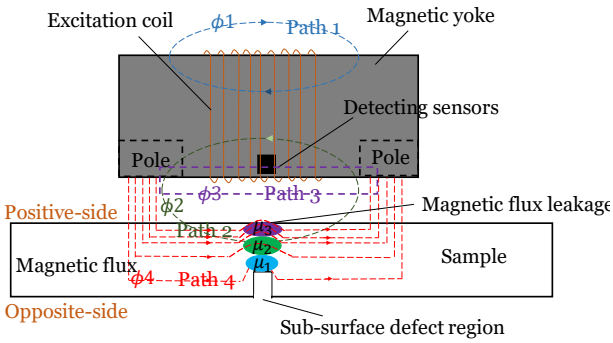

Fig. 2 The magnetic path between the proposed probe and sample.

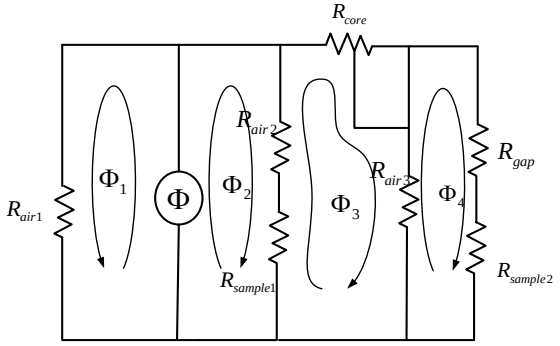

Fig. 3 Model of equivalent circuit.

In Fig. 3, according to Ohm's law in magnetic flux circuits [36], the magnetic flux Φ is inversely proportional to the magnetoresistance R, and the product of them is magnetomotive force F.

$$F = NI = \Phi R \tag{1}$$

where I presents as excitation current of the coil, and N denoted as the turns of the coil.

$$R_{p1} = R_{air1} = \frac{l_1}{\mu_0 A_{air1}} \tag{2}$$

$$R_{p2} = R_{air2} + R_{sample1} = \frac{l_2}{\mu_0 A_{air1 gap}} + \frac{l_2'}{\mu_{sample} A_{sample1}} \tag{3}$$

$$R_{p3} = R_{core1} + R_{air3} = \frac{2l_3}{\mu_{core} A_{core1}} + \frac{l_3'}{\mu_{air} A_{air3}} \tag{4}$$

$$R_{p4} = R_{core2} + R_{gap} + R_{sample2} = \frac{2l_4}{\mu_{core} A_{core2}} + \frac{l_{gap}}{\mu_0 A_{gap}} + \frac{l_4'}{\mu_{sample} A_{sample2}} \tag{5}$$

where μ_0, μ_{core}, and μ_{sample} are permeability of the air, magnetic yoke and sample, respectively, A_{air1}, A_{air2}, $A_{sample1}$, A_{air3}, A_{core1}, A_{core2}, A_{gap} and $A_{sample2}$ are the cross sectional area of the air in the Path1, the air, the sample in the Path2, the air, the core in the Path3, the core, the gap, the sample in the Path4, respectively.

For ferromagnetic material, due to high permeability, $\mu_{core} > \mu_{sample} \gg \mu_{air}$, the flux leakage in the air is small. Most flux is flowing into the sample, and forming a closed magnetic loop to magnetize sample. For non-ferromagnetic material, due to $\mu_{core} > \mu_{sample} \approx \mu_{air}$, the magnetic flux which flow into Path1 and Path 3 is large. In particular, the shorter the path, the greater the magnetic flux as this is independent of sample parameter.

C. *Mathematical model of electromagnetic detection*

By using the magnetic flux analysis, multi-physics technique can now be integrated into the defect detection and applications. The distribution of magnetic flux is mainly affected by the permeability of sample, and the eddy current disturbance is mainly influenced by the discontinuous conductivity of the sample. Although the excitation mode of AC-MFL and MFL are identical, the detection mechanism is different.

1) *Mathematical model of electromagnetic induction*

ACFM detection method is mainly based on the principle of electromagnetic induction [37]. The excitation system of the probe can be composed of coil or yoke, and the purpose is to excite uniform current field. As surface defects exist, the induced current cannot pass through the defect due to the large electrical resistivity of the defect. Thus, it will flow from the end and the bottom of the defect. According to Maxwell's Eq (1) and (2), if the alternating current field is perpendicular to the defect, the disturbance is most significant where a corresponding distorted magnetic field will be produced. The magnetic sensor between two pole shoes can detect the vertical and horizontal magnetic flux components, as shown in the Fig. 4. To calculate the disturbance of electromagnetic field caused by defects conveniently, magnetic vector potential $\vec{A}$ is introduced, as shown in Eq. (6). According to the principle of electromagnetic induction, the magnetic vector potential $\vec{A}$ satisfy Laplace law (7). There are defects on the surface of the specimen, magnetic vector potential $\vec{A}$meets the Eq. (8).

$$\vec{B} = \nabla \times \vec{A} \tag{6}$$

$$\frac{\partial^2 \vec{A}}{\partial X^2} + \frac{\partial^2 \vec{A}}{\partial Y^2} + \frac{k\mu_0}{\mu} \frac{\partial \vec{A}}{\partial Z} = 0 \qquad z = 0 \tag{7}$$

where $\vec{B}$ is the magnetic induction density, $\vec{A}$ is the magnetic vector potential, μ_0 is the air permeability, μ refers to the permeability of the material, among $|k| = \sqrt{\frac{2i}{\delta^2}}$, and δ indicted the skin depth of test piece $\delta = \sqrt{\frac{2}{\mu\sigma\omega}}$.

$$\frac{\partial^2 \vec{A}}{\partial X^2} + \frac{\partial^2 \vec{A}}{\partial Y^2} + \frac{k\mu_0}{\mu} \frac{\partial \vec{A}}{\partial z} = \left(2 + \frac{ck\mu_0}{\mu}\right) \frac{\partial^2 \vec{A}}{\partial Z^2} \delta(Y) \qquad z = 0 \tag{8}$$

The boundary conditions of the surface magnetic field Z are distinct for different materials, for ferromagnetic materials, $\mu \gg \mu_0$, $\frac{\mu_0}{\mu} \approx 0$, Eq. (9) is derived from the Eq. (8), and for non-ferromagnetic materials, $\mu \approx \mu_0, \frac{\mu_0}{\mu} \to \infty$, Eq. (10) is derived from the Eq. (8).

$$\frac{\partial^2 \vec{A}}{\partial X^2} + \frac{\partial^2 \vec{A}}{\partial Y^2} = 2 \frac{\partial^2 \vec{A}}{\partial Z^2} \delta(Y) \qquad z = 0 \tag{9}$$

$$\frac{k\mu_0}{\mu} \frac{\partial \vec{A}}{\partial z} = \left(2 + \frac{ck\mu_0}{\mu}\right) \frac{\partial^2 \vec{A}}{\partial Z^2} \delta(Y) \qquad z = 0 \tag{10}$$

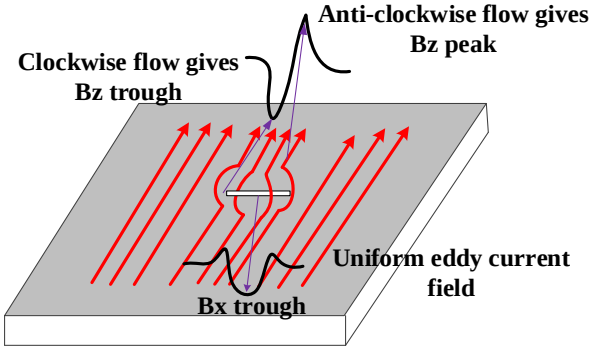

Fig. 4 ACFM principle around a crack.

2) *Multiphysics coupling detection method*

On the basis of ACFM detection, the coupling sensing of AC-MFL is further proposed to realize the combination of multiple detection methods. The essence of the AC-MFL detection method is the discontinuity of the material, and "squeezed" out the magnetic flux into the air [38]. Due to the saturation of the magnetic field on the surface of the specimen, when the surface defects are detected, on the basis of Eq. (11) and (12), the disturbed secondary alternating magnetic field B_{dis} and a small amount magnetic flux B_{MFL} will be produced concurrently, which

are the ACFM and AC-MFL respectively. In particular, the AC-MFL has the same principle for subsurface defect detection, the compressed curved magnetic field lines will squeeze to the surface of the specimen. The leakage flux "squeezed" out of the subsurface defect is relatively weak, and therefore high sensitivity and low hysteresis TMR2701 sensor is used for weak magnetic signal measurement. The BH curve of ferromagnetic materials is not only non-linear but also a non-single value function. In addition, according to Eq. (13) and (14), magnetic intensity H and magnetic induction density B cannot be uniquely determined. It is not only related to the H at that time, but also influenced by the previous magnetization state (History).

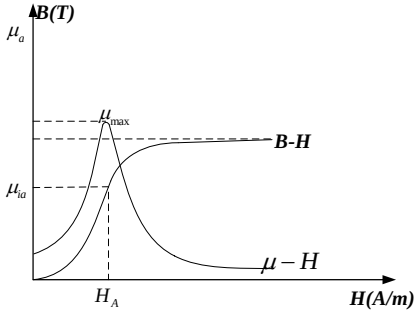

Fig. 5 $B-H$ and $\mu-H$ curve.

$$B_{surface} = B_{dis} + B_{MFL} \quad (11)$$

$$B_{sub-surface} = B_{MFL}{}' \quad (12)$$

where B_{dis} and B_{MFL} are secondary disturbed magnetic field and magnetic flux leakage produced by surface defect, respectively. $B_{surface}$ refers to the magnetic sensor detection signal, $B_{MFL}{}'$ is magnetic flux leakage produced by sub-surface defect.

$$B = \mu_0(H + M) \quad (13)$$

$$\mu = f(H) \quad (14)$$

where μ_0 is the air permeability, a constant, M is the strength of magnetization, H refers to the magnetic field intensity.

According to Fig. 5, when the magnetic field intensity H of ferromagnetic material reaches to the saturation state H_{max}, the permeability of the specimen the different μ reaches to different region, $\mu_{sample} \gg \mu_1 \geq \mu_2 \geq \mu_3$. There will improve penetrating capability of initial magnetic field. At this time, the penetration formula does not apply to the penetration situation under the magnetization state, and the existing subsurface defects hinder the magnetic flux lines flow. It squeezes out of the positive side of the specimens while magnetic leakage field B_{mfl} can be shown in Fig. 2.

III. Simulation And Analysis

To verify the feasibility of the proposed electromagnetic coupling mechanism, several numerical simulation experiments are carried out by using COMSOL Multiphysics 5.5a platform. The geometric sketch of the model is shown in the Fig. 6 (a) - (b), which is top view and side view, respectively. The geometric model is mainly composed of copper, Mn-Zn ferrite core and sample, respectively. The physical properties and geometric parameters of the material are listed in Table I and Table II, respectively, the distance (lift-off) between the excitation structure and the specimen surface is 1mm. In the experiments, considering the nonlinearity of sample, it is necessary to set up BH curve of the material. In addition, the physical field of sample is set to the effective BH curve. The study is set to the frequency domain analysis, the number of turns of the coil are 120, the excitation voltage is 16V and the frequency is 4kHz.

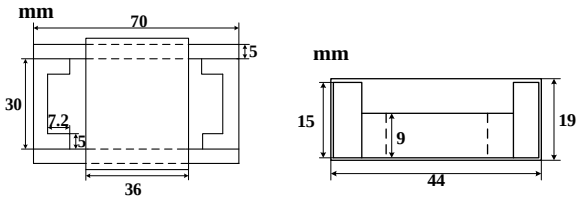

(a) Top view. (b) Side view.

Fig. 6 Geometric sketch of the proposed structure model.

Table I Parameter of simulation model.

Parameters	Driver coil	Magnetic yoke	sample
Conductivity	5.99e7	1e-12	5.5e6
Relative permeability	1	4000	190
Turns	120	×	×

Fig. 7 illustrates space diagram with the defect scanning process. Due to the particularity of the excitation structure, it is geometrically symmetrical and has strong magnetic gathering ability. As a result, both uniform current field and magnetic flux field will be produced on the specimen.

Table II Test piece parameters

Parameters		Length (mm)	Width (mm)	Depth (mm)	Angle (°)
45#steel sample		700	400	10	×
The different angle defect	Surface	10	2	4	90
	Surface	10	2	4	45
	Surface	10	2	4	0
The different depth defect	Surface	10	2	4	90
	Sub-surface	10	2	2	90

As shown in Fig. 8. In contrast to defect and non-defect regions, it demonstrates the different induction current distribution and the magnetic flux distribution. The defect detection results are obtained by changing flux density and current density.

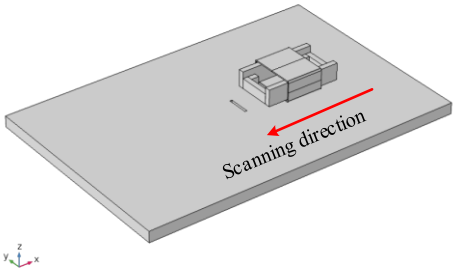

Fig. 7 Space diagram with the defect scanning direction.

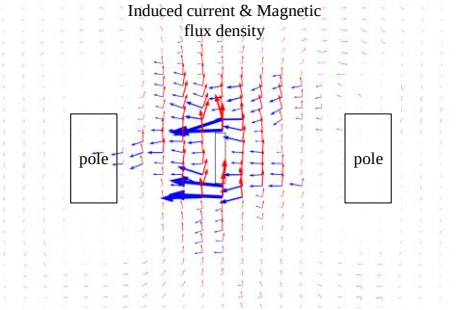

Fig. 8 Distribution of current field and magnetic flux field.

The proposed magnetic flux circuit model is mainly applied to describe the magnetic flux distribution. Through the analysis of magnetic circuit, the fusion ability of magnetic flux leakage detection and AC electromagnetic field detection can be improved. The specific magnetoresistance and flux parameters are approximated in finite element analysis. The parameters are shown in the

Table III.

Table III Magnetoresistance and flux parameters approximation

ϕ (uWb)				R (H)		
ϕ_1	ϕ_2	ϕ_3	ϕ_4	R_{sample}	R_{core}	R_{air}
13.5	58.1	84.5	129	0.92	0.47	1870
Note: $R_{sample} = R_{sample1} + R_{sample2}$; $R_{air} = R_{air1} + R_{air2} + R_{air3}$						

The optimal position of the magnetic sensor is determined according to the maximum disturbance of the detectable defect. Once it is located in the center of yoke, the transformation of the electromagnetic disturbance field is the largest, which can be verified by simulation. The simulation results can be shown in Fig. 9.

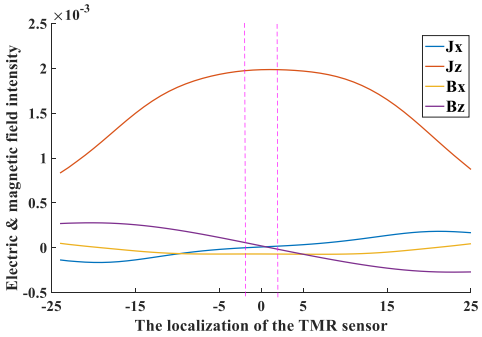

Fig. 9 Relationship between magnetic sensor position and current density and magnetic flux density distribution

a) Mechanism analysis of different angle defect detection

In analyzing the electromagnetic coupling mechanism of ACFM and AC-MFL technique, it is observed that in accordance to the characteristics of ACFM inspection, when the alternating current field is perpendicular to the defect direction, the disturbance of current field is the largest, and the signal can be detected with high SNR. The detection characteristic of the AC-MFL is that when the magnetization direction is perpendicular to the defect, the magnetic flux leakage above the defect is the largest as the signal is easily captured. Using the orthogonal characteristic of magnetic flux leakage field and AC electric field, the defects with different angles can be detected.

The simulation is implemented to study defect detection of different angles. The length, width and height of defects are10mm, 2mm, 4mm, respectively. The inclination angles are 90 °, 45 ° and 0 °, respectively. Due to the magnetic induction B, it includes not only ACFM signal, but also AC-MFL signal. Therefore, we evaluate the detection ability of the fusion of the two detection methods by observing the changes of magnetic field disturbance caused by defects from different angles. The simulation results are shown in Fig. 10 (a) - (b), and the sensitivity of defect detection from different angles is as high as 0.85. This is verifying the reliability of the proposed method.

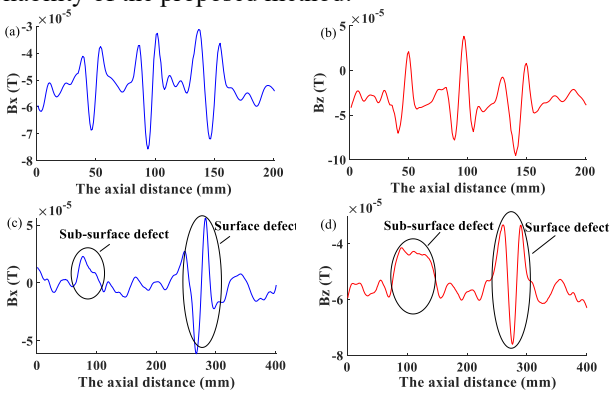

Fig. 10 Different surface defect angle detection(a) Bx. (b) Bz. Subsurface and surface defect detection (c) Bx. (d) Bz.

b) Analysis of detection mechanism of surface and subsurface defects

In order to further verify the detection ability of the proposed sensor structure, simulated experiment is carried out on the subsurface defect detection of sample. This is mainly based on the AC-MFL detection mechanism. According to the proposed theoretical method, when a probe passes over subsurface defect through the magnetization of the specimen, the surface of specimen squeezed out a small amount of leakage flux which can be captured. In the simulated experiment, surface and subsurface defects simultaneously exist on the sample, and the defect is perpendicular to the magnetization field. The simulation results are shown in Fig. 10 (c)-(d). The characteristics of subsurface and surface defect signals are just opposite to each other. The surface defect signal corresponds to the peak value, and the subsurface defect corresponds to the valley value. In particular, the disturbance signal generated by the subsurface defect is mainly caused by magnetic flux leakage. Since that ACFM is limited by the skin depth, and the penetration ability of current field will also be limited. The interference magnetic field produced by surface defects is influenced by both AC-MFL and ACFM simultaneously.

IV. EXPERIMENTAL SET-UP AND VALIDATION

To validate the feasibility of the proposed model and detection structure, the proposed physics coupling sensing system is implemented. The experimental studies and results are analyzed in detail.

a) Experiment platform set up

The developed experimental platform is shown in Fig. 11. The probe structure is composed of a magnetic yoke, AC coils, TMR sensors, and detection circuit. All components are packaged in a self-designed carbon brazing device. The excitation system is mainly consisted of AFG3051C signal generator and DPA-1698 instrument amplifier. The power structure is composed of a X-Y-Z workbench and an auxiliary power while the moving worktable can be used to control the probe to scan at a constant speed. The acquisition device is comprised of NI USB-6366 DAQ card and laptop, which is used to collect and process data.

The detection circuit is composed of high sensitivity magnetic sensors and AD620 operational amplifier circuit. The selected magnetic sensor has advantages of high sensitivity and small hysteresis, which is used to pick up the disturbed magnetic signal caused by defects. The hysteresis level of the magnetic sensor is 23.6A/m under the range fitting of ±1194.3A/m linear region. Considering that the disturbance signal ratio is weak, the amplification filter circuit is designed to process the collected signal, and the entire conditioning circuit is integrated.

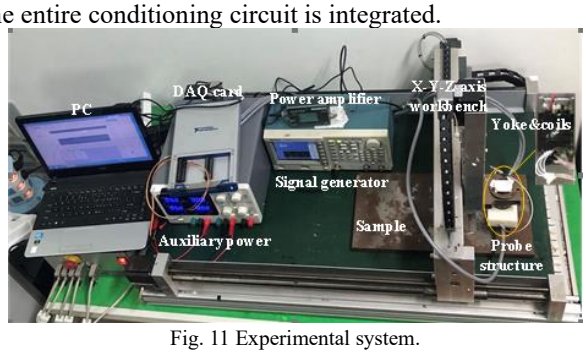

Fig. 11 Experimental system.

b) Description of tested Samples

The photographs of the isotropic samples are shown in Fig. 12. There are surface defects on the specimen (a)-(b). Fig. 12 (a) includes notches with different angles from 15° to 75°. They are identical lengths, widths and depths, with different depths from 1mm to 6mm of identical lengths, widths and angles, with different widths from 1mm to 6mm of identical lengths, angles and depths. Fig. 12 (c) presents four types of surface defects in the specimen with a thickness of 10mm. They are different angles, diameters, depths, widths, respectively. Fig. 12 (e) presents subsurface and different surface defects with different depths of identical lengths, widths and angles.

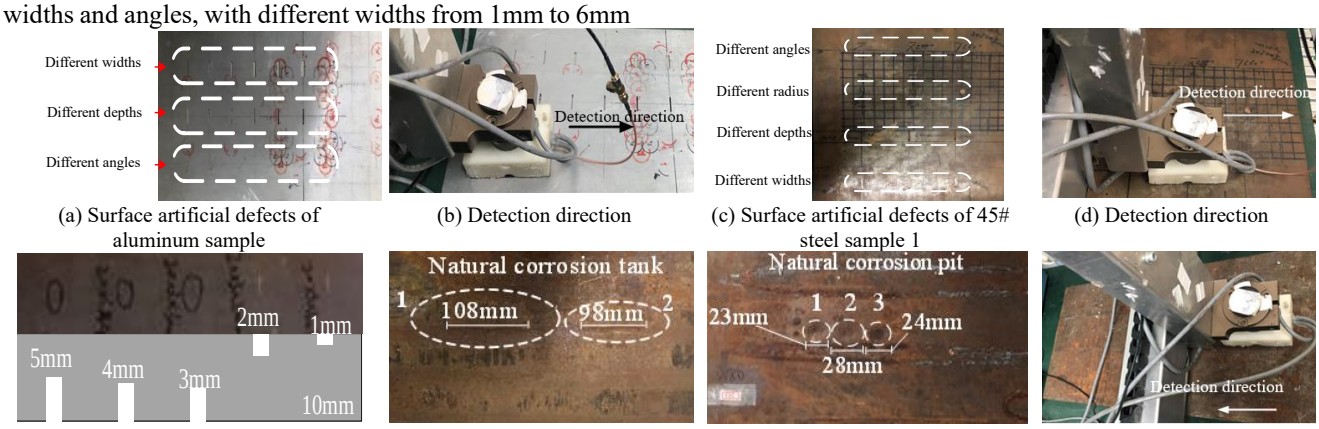

(a) Surface artificial defects of aluminum sample

(b) Detection direction

(c) Surface artificial defects of 45# steel sample 1

(d) Detection direction

(e) Sub-surface and surface artificial defects of 45# steel sample 2

(f) Natural corrosion tank of X80 steel of pipe

(g) Natural corrosion pit of X80 steel of pipe

(h) Detection direction

Fig. 12 Description of specimens with artificial and natural defects.

c) Results Analysis

The experimental parameter settings are described as follow: (1) In all experiments, the coil of excitation parameters is set to 8Vpp, 4kHz and the power amplifier is used to drive the probe. the number of coil turns is 120, and the wire diameter of coil is 0.20mm. (2) The distance of the proposed probe and samples is 2mm. (3) The scanning speed of the proposed probe is 20mm/s. (4) The sample rate of the NI-6226 data acquisition card is set to 40kHz.

In order to quantitatively evaluate the defect detection capability of the proposed system, the size range of defects is analyzed by calculating the sensitivity parameter S, which can be expressed as follows:

$$S = \left| \frac{Max(V_{Defect} - V_{(Defect-free)})}{V_{(Defect-free)}} \right| \tag{15}$$

where V_{Defect} and $V_{(Defect-free)}$ respectively represent the output value of the TMR sensor with and without defects, S represents the sensitivity at the defect.

Due to the bias and low signal-to-noise ratio of the original data, a Butterworth fourth-order band-pass filter is used to process the original data to improve the defect detection sensitivity and reduce the signal bias, the Butterworth bandpass filter is selected with cutoff frequency range (3.6-4.4kHz). Discrete-time analytic signal (AS) is used to extract the data envelope. The signal processing process is shown in the Fig. 13.

The data frequency sampling is 40kHz, and the cutoff frequency is selected within the range of 3.6 to 4.4khz, the passband attenuation smaller than 3dB, and the attenuation at 3.4kHz and 4.6kHz is more than 18dB. The 4th order Butterworth bandpass filter has been designed for the above specification. The specific steps are described as follow:

(1) Determining the indicators of the filter: upper cut-off frequency of passband, lower cut-off frequency of passband, upper cut-off frequency of stopband, lower cutoff frequency of stopband, maximum attenuation in passband and minimum attenuation in stopband.

(2) Using $\omega = \frac{2}{T}\tan(w/2)$ digital boundary of bandpass digital filter $H(z)$. The boundary frequencies of bandpass analog filter $H(s)$ are mainly passband cut-off frequencies $wp1$ and $wp2$; Conversion of stopband cut-off frequencies $ws1$ and $ws2$. For the convenience of calculations, the bilinear transformation method is generally T = 2s.

(3) Using the low-pass to band-pass frequency conversion formula $\lambda = ((\omega^2) - (\omega_0{}^2))/B \cdot \omega)$ to convert the analog band-pass filter index to the analog low-pass filter index.

(4) Designing the analog low-pass prototype filter. With the help of Butterworth filter design method, the transfer function $Ha(s)$ of analog low-pass filter is obtained.

(5) Calling lp2bp function to convert analog low-pass filter into analog band-pass filter.

(6) The analog bandpass filter $Ha(s)$ is transformed to a digital bandpass filter $H(z)$ by bilinear transformation method.

The analytical signal corresponding to a real signal is obtained by the Discrete Fourier transform (DFT) and its inverse DFT, and then the envelope of the signal is obtained from the modulus of the signal. The main steps are as follows:

(1) The DFT is performed on the filtered signal $x(n)$, the corresponding frequency domain signal $X(i)$ can be obtained, where $n, i \in \{0,1,2,\ldots,N-1\}$;

(2) The DFT of discrete-time AS of x(n) is defined as

$$Y(i) = \begin{cases} X(i) & for\ i = 0 \\ 2 \cdot X(i) & for\ i = 1,2,\ldots,\frac{N}{2} - 1 \\ X(i) & for\ i = \frac{N}{2} \\ 0 & for\ i = \frac{N}{2} + 1,\ldots,N-1 \end{cases} \tag{16}$$

(3) The complex discrete-time AS $y(n)$ corresponding to $x(n)$ is obtained by the inverse DFT of $Y(i)$;

(4) The modulus $y(n)$ of the complex AS $|y(n)|$ corresponds to envelope of discrete real signal $x(n)$.

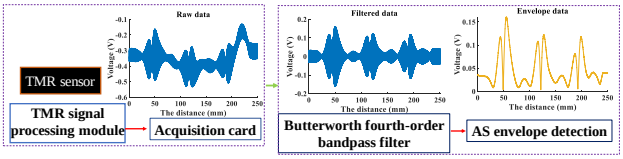

Fig. 13 Signal processing process

1) Detection results in aluminum sample

The detection results of different types of defects in aluminum sample are analyzed by using the proposed detection system. Since the test specimen is non-ferromagnetic material, the magnetic flux leakage will not occur at the defect region, while only ACFM detection takes the main role in detection. The moving direction of the probe is approximately parallel to the alternating electromagnetic field as this is perpendicular to the defect direction. The test results are shown in Fig. 14 (a) and (b), respectively. Firstly, all defects on the aluminum plate can be detected by the proposed excitation configuration. Secondly, when the scanning direction of the probe and the defect have an angle of 15°, the signal characteristics of Bx and Bz are obvious in which this is consistent with the signal characteristics of the ACFM detection mechanism. By analyzing the sensitivity of different types of defects in Table IV, it can be found that in the defect detection of non-ferromagnetic materials, Bz changes significantly with the defect angle, and the minimum sensitivity is 0.47. Both Bx and Bz have rare effect on the change of defects at different depths. When the depth of the defect is 1mm, there is still a higher sensitivity of 0.77.

2) Detection results of defects in 45# steel sample

The experimental parameters and the experimental environment are the same set as the test in aluminum plate. Since 45#steel sample is ferromagnetic material, both ACFM and AC-MFL methods can take role in defect detection, the fusion of multiple detection methods has significantly improved the detectability of different types of defects. On the one hand, the proposed probe configuration can detect different types of surface defects as AC-MFL can be sensitive to circumferential defects and axial defects. It is realized that high-sensitivity detection of defects at different angles, as shown in Fig. 14(d) and Fig. 14 (e), respectively. According to Table V, it is found that the proposed probe has high sensitivity to different depths and different angles as well. Bz is approximately linear with the relationship of different defect depths. When the surface defect depth is 8mm, the detection sensitivity is 2.62. At the same time, it has high sensitivity for subsurface defects. When the distance of the subsurface defect is 7mm, the sensitivity can still maintain significantly high at 0.15.

On the other hand, AC-MFL detection methods can be used to inspect sub-surface defects, which is complementary to the ACFM technology. It can be used to identify both surface and sub-surface defects and improve the detectability. To simplify interpretation, two groups of experiments have been tested. In the first group, the specimens of Fig. 12(c) are turned over, and the third column of subsurface defects with different depths is detected, the results are shown in Fig. 15(a). In the second group, the specimens with both surface defects and subsurface defects are detected, and the results are shown in Fig. 15(b). The reason why the DC component is not eliminated is caused by several factors. In addition to the influence of geomagnetic field, ferromagnetic materials generally have remanence, which will produce DC bias to the signal. Concurrently, the AD620 amplification chip will amplify the magnitude of the bias. In particular, eliminating the DC component might not improve the detection effect due to different test samples. This extra process might increase the circuit complexity and possibly lose signal when conduct in the different test objectives. According to the analysis of Fig 15 (b), when there are surface defects, both Bx and Bz of the signals occur fluctuate simultaneously. When there are only subsurface defects, Bz signal jumps as Bx has no noticeable change.

3) Detection results of natural corrosion defects

In order to further verify the detection ability of the proposed probe, irregular natural defect specimens are used. Due to the complex surface condition of the specimens, the traditional detection structure is not suitable to detect the specimen with complex surface conditions. The proposed probe has high sensitivity for natural defect detection. The detection results are shown in Fig. 16(a)-(b), and the number of Natural corrosion tank and Natural corrosion pit of X80 steel of pipe can be judged according to the peak number of the signal, it is tank 1, tank 2, pit 1 pit 2 and pit 3, respectively. In Table VI, it is found that the proposed probe has high sensitivity for natural corrosion tanks and natural corrosion pit detection. It can not only quantify the number of defects, but also evaluate the size of defects to a certain extent.

Table IV Detection results of aluminum sample

Parameters of surface defect of aluminum sample						Bx sensitivity	Bz sensitivity
Defect angle (°)						0.02, 0.02, 0.03, 0.03, 0.03	0.47, 0.75, 1.00, 1.04, 0.90
15	30	45	60	75			
Defect depth (mm)						0.03, 0.04, 0.03, 0.03, 0.03, 0.03	0.77, 1.00, 1.01, 0.95, 0.95, 0.95
1	2	3	4	5	6		

Table V Detection results of 45#steel sample.

Parameters of surface defect of 45# steel sample1					Bx sensitivity	Bz sensitivity
Defect angle (°)					0.04, 0.04, 0.06	0.86, 0.46, 0.86
30	45	60				
Defect depth (mm)					0.09, 0.09, 0.10	1.88, 1.98, 2.62
4	6	8				
Sub-surface defect depth of 45# steel sample1(mm)					0.02, 0.02, 0.02	0.26, 0.59, 1.05
4	6	8				
Parameters of sub-surface defect depth of 45# steel sample2					0.04, 0.03, 0.03, 0.06, 0.07	0.11, 0.11, 0.15, 0.73, 0.88
Sub-surface defect depth (mm)			Surface defect depth (mm)			
5	4	3	2	1		

Table VI Detection results of Natural defect X80 steel.

Natural corrosion tank (mm)			Bx sensitivity	Bz sensitivity
108		98	0.01, 0.02	1.34, 0.60
Natural corrosion pit (mm)			0.00, 0.01, 0.01	0.70, 2.87, 1.84
23	28	24		

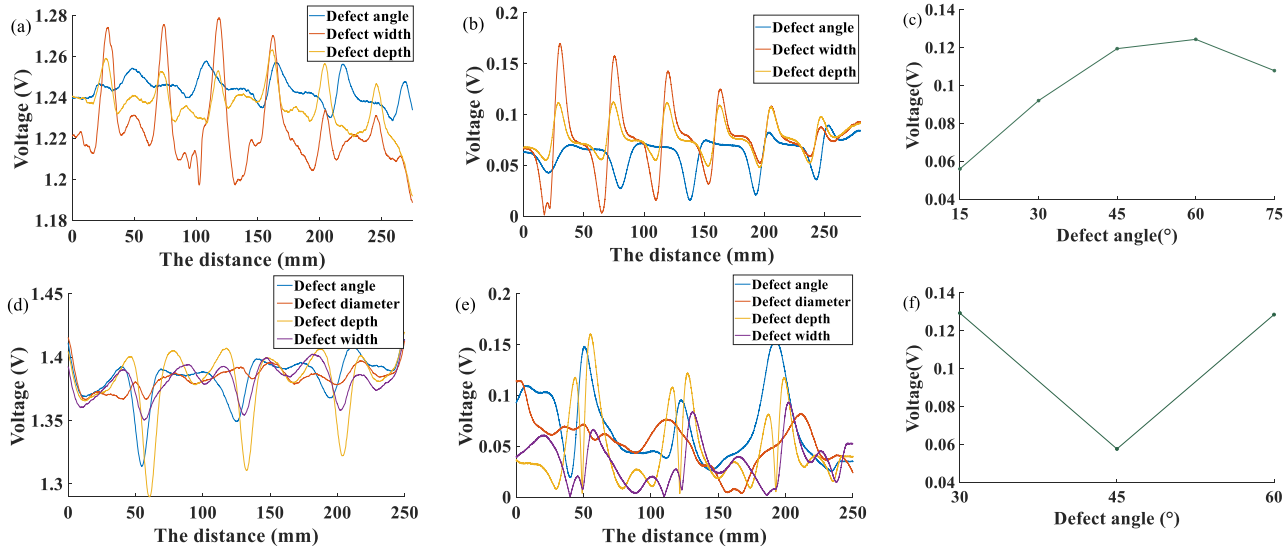

Fig. 14 (a), (b) are the horizontal component Bx and vertical component Bz envelope value of different defect angle, defect width, different defect depth in aluminum plate. (c) is the relationship between the defect angle and the envelope peak value in aluminum plate. (d), (e)are the Bx and Bz envelope value of different defect angle, defect diameter, defect width, different defect depth in the 45# steel. (f) is the relationship between the defect angle and the envelope peak value in the 45# steel.

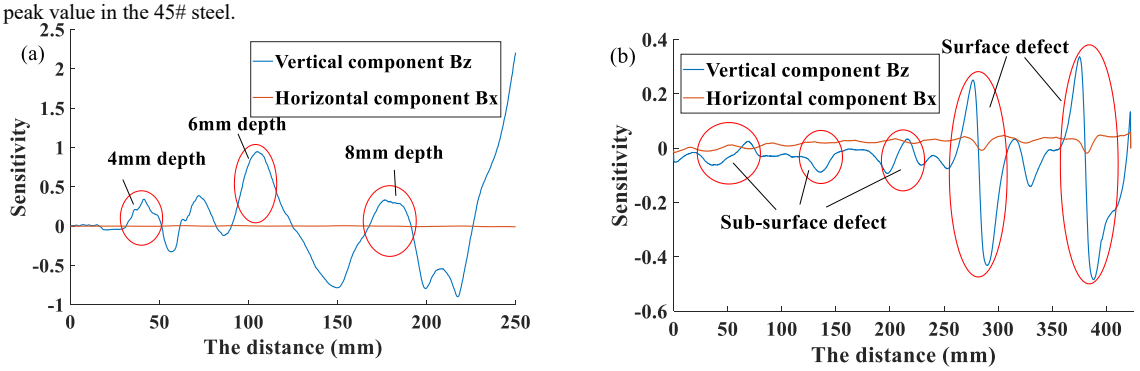

Fig. 15 (a) refers to sub-surface artificial defects detection results with different depth. (b) presents sub-surface and surface artificial defects detection results with different depth.

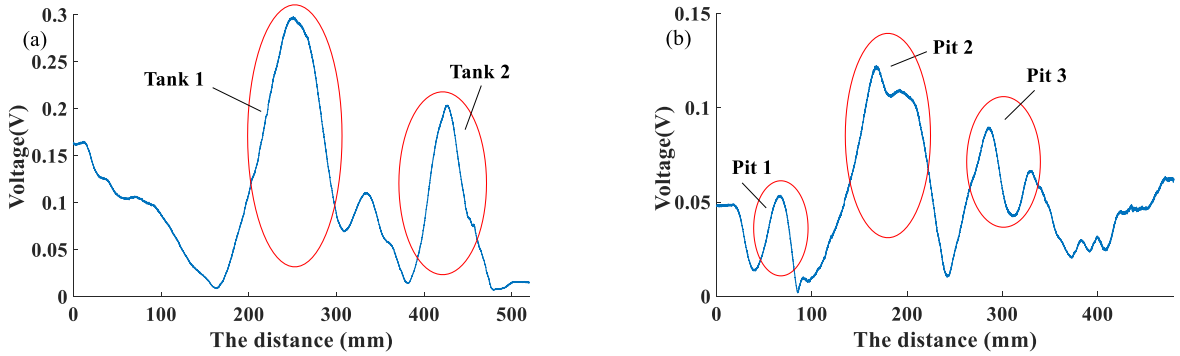

Fig. 16 (a) Natural corrosion tank detection results. (b) Natural corrosion pit detection results.

4) Comparison

In order to verify the advantages of the proposed probe, we compared the traditional U-shaped yoke probe and planar eddy current probe structures. The U-shaped yoke probe was designed referring to ACFM probes as reported in [9]. The planar probe was designed referring to EC probes as reported in [28]. The specific experimental setup is shown in Fig. 17. Fig. 17(a) shows that the probe is controlled by the 6-Axis Manipulator to scan the pipeline. The scanning speed is 20mm/s. and the scanning distance is 600mm. Fig. 17 (b) shows the experimental state when the inner side of the pipe is coated with liquid such as magnetic suspension. Fig. 17 (c) shows the inspection on the outside of the pipeline. the metrics of different probes are listed in Table VII. The experiment is divided into the comparison of the detectability and sensitivity of the probe to different pipeline defects. Fig. 18 shows different probe structures.

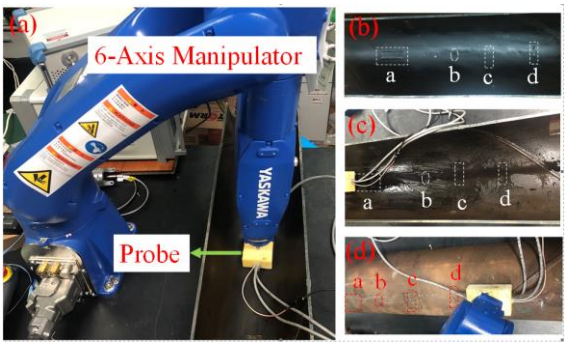

Fig. 17 Schematic of pipe inspection Testing system.

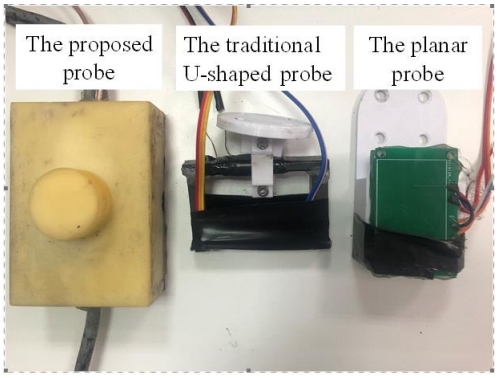

Fig. 18 Probes structure

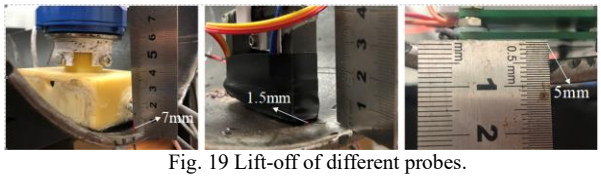

Fig. 19 Lift-off of different probes.

Table VII Comparison of the probes

The probes structure	The proposed probe	Traditional U-shaped yoke probe	Chen (2021) [28]	
Sensor	TMR	TMR	Coil	
Excitation method	Yoke & Coil	Yoke	Coil	
Excitation frequency	4kHz	4kHz	2MHz	
Turns	120	150	20	
Length (mm)	70	67	48	
Width (mm)	44	12	30	
Height (mm)	19	44	10	
Type and approximate size of defects (mm)	The axial defect (a)	The square defect (b)	The circumferential defect (c)	The circumferential defect (d)
	76×23.7×1.8	7×6×1.6	2×45×2	8×36×3

a) Sensitivity and functional comparison experiment

Three different types of probe structures are used to detect different types of defects on the inner side of the pipeline inspection. The contact between the probe and the inner wall of the pipe is shown in Fig. 19. The mechanical arm controls the three probes to move at the same speed, and the detection results are shown in Fig. 20.

In order to facilitate the benchmarking of defect location and signal characteristics, the Bx reference voltage is reduced by 2.1V.

By comparing Fig. 20 (a), (b) and (c), it can be observed that defects #a and #d on the inner side of the pipeline can be identified by the three probes. Defect #b can be detected by the proposed probe and planar probe through feature analysis. The traditional U-shaped probe cannot identify defect #b. The proposed probe can clearly identify the sub-surface defect #c while the planar probe fails to detect defect #b. The test results show that the proposed probe has high sensitivity and SNR in detecting small defects and sub-surface defects.

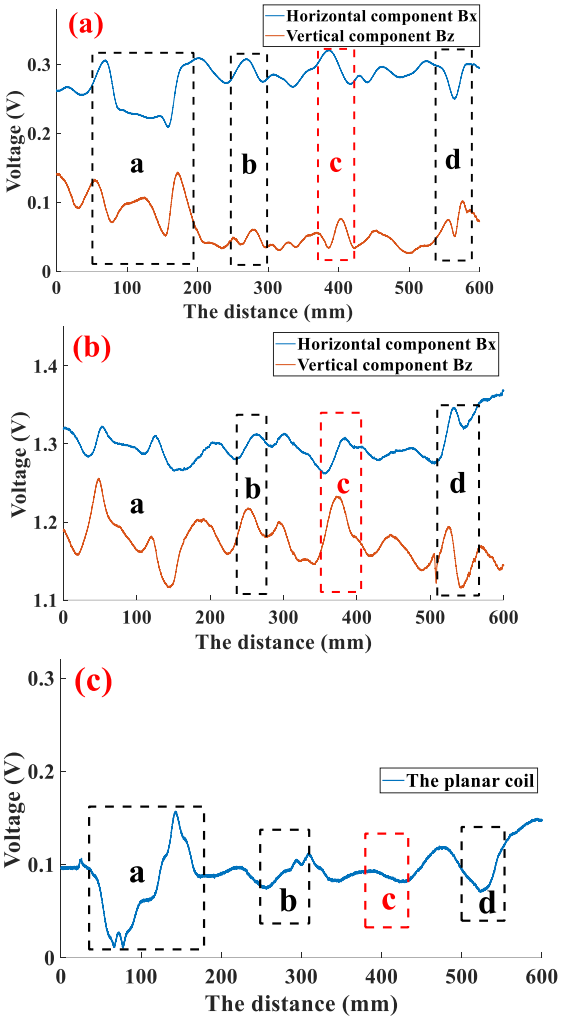

Fig. 20 Test results of different types of probes inside the pipeline. (a) The proposed probe. (b) The traditional U-shaped yoke probe. (c) The planar probe.

The evaluation is conducted by normalizing the experimental results due to the balance of different scale range of the different probe as shown in the formula 1, and then solve the corresponding sensitivity. The results are shown in the Table VIII.

$$Normalization = \frac{x - min(x)}{max(x) - min(x)} \tag{16}$$

$$SNR = 20\, log_{10}\left(\frac{V_{aD}}{V_{aN}}\right)[dB] \tag{17}$$

where V_{aD} and V_{aN} are average voltage variation in defective and non-defective regions of tested piece, respectively.

Table VIII Index comparison results

Probe type for pipeline inspection	Proposed probe				Traditional U-shaped yoke probe				Chen (2021)			
Inner pipeline defect inspection	a	b	c	d	a	b	c	d	a	b	c	d
Sensitivity (Bx, Bz or Pcb coil)	1.2 2.4	0.5 0.7	0.6 1.1	1.3 0.7	1.1 2.2	0.04 0.3	0.2 0.9	1.0 1.1	1.9	0.5	0.03	0.64
Efficacy (Detectability)	D4/4				3/4				3/4			
Precise	√	√	√	√	√	×	√	√	√	√	×	√
(Bx+Bz or coil) SNR (dB)	11.1	1.6	4.6	6.0	10.4	-9.4	0.8	6.4	5.6	-5.8	-30	-3.9

Note: √ and × indicates detected and not detected respectively

The defect detection efficiency is calculated according to the detection ratio of different types of defects. The detection efficiency of the proposed probe is quantified in terms of detecting circumferential defects, axial defects, circular small defects and sub-surface defects.

In the actual pipeline detection, we are more concerned about the detection of sub-surface defects as they are not easy to detect while general detection methods fail to deliver acceptable detection performance and thus lead to undetected defect that compromise the pipeline safety. Next, we carry out comparative experiments on the types of probes that can detect sub-surface defects in complex environments.

b) Complex detection environment experiments

Case1: Detection comparison of complex specimen structure

The experiment verifies the adaptability of the proposed probe to different detection structures. The experimental setting is consistent with case 1. By reversing the pipeline in Fig. 17 (a), the detection experiment is carried out on the outside of the pipeline. The pipe condition is shown in Fig. 17 (d), and the experimental results are shown in Fig. 21.

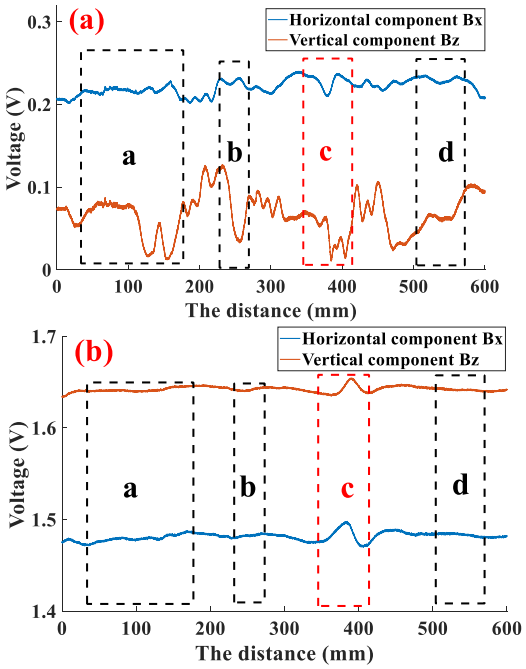

Fig. 21 Test results of different types of probes outside the pipeline. (a) The proposed probe. (b) The traditional U-shaped yoke probe.

By comparing Fig. 21(a) and (b), the external detection is analyzed. The proposed probe can detect three defects #a, #b, #c. In terms of the defect #d, the detection sensitivity is limited due to the sub-surface defect depth being too small, and less magnetic field leakage on the pipeline surface. The traditional U-shaped probe can only detect defects #c. Thus, this confirm the adaptability and detectability of the proposed probe are better than the traditional U-shaped probe. Specific results are shown in Table IX.

Table IX The external detection results

Probe type for pipe inspection	The proposed probe				Traditional U-shaped yoke probe			
Outer pipeline side inspection	a	b	c	d	a	b	c	d
Sensitivity	1.0	0.7	1.5	0.2	0.1	0.0	1.5	0.1
Efficacy	3/4				1/4			
Precise	√	√	√	×	×	×	√	×

Case2: Complex surface condition of specimen structure

In addition, in order to further verify the adaptability of the proposed probe to complex environment, a large amount of magnetic suspension is coated on the pipe surface to simulate the complex surface situation in the actual pipeline. Other experimental settings are consistent with case 1. The experimental results are shown in Fig. 22. Compared with the pipeline with clean surface, the detection sensitivity of the pipeline coated with magnetic suspension is reduced by about 0.2. The specific parameters are shown in the Table X, however, it does not affect the actual defects detection of pipeline. The experimental results show that the proposed probe structure is rarely affected by the degree of surface cleanliness and has great adaptability to complex environment.

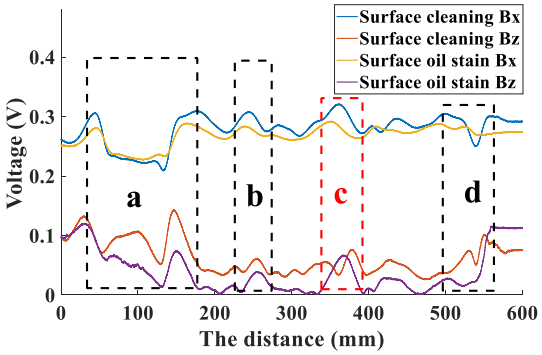

Fig. 22 shows the comparison results of pipeline surface cleaning and oil stand inspection

Table X results of Surface cleaning and Surface oil stain pipeline

Probe type for pipe inspection	The proposed probe (Surface cleaning)				The proposed probe (Surface oil stain)			
inner pipeline side inspection	a	b	c	d	a	b	c	d
Sensitivity	2.4	0.7	1.1	0.7	2.2	0.5	0.9	0.5
Efficacy	4/4				4/4			
Precise	√	√	√	√	√	√	√	√

IV. CONCLUSION AND FUTURE WORK

This paper has proposed a novel electromagnetic diagnostic system that couples the ACFM with MFL sensing structure. The theoretical analysis of ACFM and AC-MFL has been presented. The corresponding simulation and experimental verification have been carried out to illustrate the feasibility and reliability of the proposed sensing structure. The following conclusions can be drawn:

1) Compared with the traditional U-shaped structure, the excitation structure saves the space size. Based on the new excitation structure, the excitation coil is fully utilized to increase the magnetization and detection sensitivity of the specimen.

2) According to the proposed electromagnetic coupling excitation structure, the advantages of ferromagnetic and non-ferromagnetic materials are compensated from the perspective of physical mechanism. The defects from different angles and subsurface defects are detected.

3) The system is used for the detection of natural defects on complex surface condition for pipeline. In particular, the number of defects can be accurately judged for serial defects, and it has strong detection ability and adaptability.

Future work will focus on quantitative detection and imaging of the pipeline defects in industrial environment.

V. ACKNOWLEDGEMENT

The work was supported by Deyuan and UESTC Joint Research Center, supported by the National Natural Science Foundation of China (No. 61971093, No. 61960206010 and No. 61527803). The work was supported by Science and Technology Department of Sichuan, China (Grant No.2019YJ0208, Grant No.2018JY0655, Grant No. 2018GZ0047) and Fundamental Research Funds for the Central Universities (Grant No. ZYGX2019J067).

REFERENCES

[1] B. Omar, Z. Djamel, and M. Hassani, "Inspections, statistical and reliability assessment study of corroded pipeline," Engineering Failure Analysis, vol. 100, pp. 1-10, 2019.

[2] Y. Sahraoui, R. Khelif, and A. Chateauneuf, "Maintenance planning under imperfect inspections of corroded pipelines," International Journal of Pressure Vessels and Piping, vol. 104, pp. 76-82, 2013.

[3] R. Pohl, A. Erhard, and H. J. Montag, "NDT techniques for railroad wheel and gauge corner inspection," Ndt & E International, vol. 37, no. 2, pp. 89-94, 2004.

[4] Razvarz, Sina, Raheleh Jafari, and Alexander Gegov. "A Review on Different Pipeline Defect Detection Techniques." Flow Modelling and Control in Pipeline Systems. Springer, Cham, 2021. 25-57.

[5] U. Ilueng, S. Shan, D. A. Foutch, S. Shan, and D. A. Foutch, "Magnetic flux leakage (MFL) technology for natural gas pipeline inspection," Ndt & E International, vol. 30, no. 1, pp. 36-36(1), 1997.

[6] N. Kasai, A. Takada, K. Fukuoka, H. Aiyama, and M. Hashimoto, "Quantitative investigation of a standard test shim for magnetic particle testing," NDT & E International, vol. 44, no. 5, pp. 421-426, 2011.

[7] Katsuhiro et al., "Consideration of multi-coil type magnetizer for detection of omnidirectional crack in magnetic particle testing," International Journal of Applied Electromagnetics & Mechanics, 2016.

[8] Shah, S. , and B. M. Mehtre . "An overview of vulnerability assessment and penetration testing techniques." Journal of Computer Virology & Hacking Techniques 11.1(2015):27-49.

[9] Li, Wei, and, Chen, Guoming, & and, et al, "Analysis of the inducing frequency of a U-shaped ACFM system," Ndt & E International, 2011.

[10] D, Topp, and Smith, "Application of the ACFM inspection method to rail and rail vehicles," Insight, 2005.

[11] I. Z. A. A, G. Y. T. A, J. W. A, S. Y. B, and D. A. C, "Quantitative evaluation of angular defects by pulsed eddy current thermography," NDT & E International, vol. 43, no. 7, pp. 537-546, 2010.

[12] O. Lucia, P. Maussion, E. J. Dede, and J. M. Burdio, "Induction Heating Technology and Its Applications: Past Developments, Current Technology, and Future Challenges," IEEE Transactions on Industrial Electronics, vol. 61, no. 5, pp. 2509-2520, 2013.

[13] Marquez, Fpg , and C. Muoz. "A New Approach for Fault Detection, Location and Diagnosis by Ultrasonic Testing." Energies 13.5(2020):1192-.

[14] Hs A, Ru A, Tua B, et al. "Small electromagnetic acoustic transducer with an enhanced unique magnet configuration." NDT & E International 110.

[15] Bin, Gao, Yunze, He, Wai, & Lok, et al. "Multidimensional Tensor-Based Inductive Thermography with Multiple Physical Fields for Offshore Wind Turbine Gear Inspection," IEEE Transactions on Industrial Electronics, 2016.

[16] Caetano, D. M. Rabuske, T. Fernandes, J. Pelkner, M. Fermont, C. & Susana, C. D. F. et al. "High-Resolution Non-Destructive Test Probes Based on Magnetoresistive Sensors," IEEE Transactions on Industrial Electronics, vol. PP, pp. 1-1, 2018.

[17] C. Yang, B. Gao, Q. Ma, L. Xie, G. Y. Tian, and Y. Yin, "Multi-layer magnetic focusing sensor structure for pulsed remote field eddy current," IEEE Sensors Journal, vol. 19, no. 7, pp. 2490-2499, 2018.

[18] L. Wei, X. A. Yuan, G. Chen, J. Ge, X. Yin, and K. Li, "High sensitivity rotating alternating current field measurement for arbitrary-angle underwater cracks - ScienceDirect," NDT & E International, vol. 79, pp. 123-131, 2016.

[19] Guo, W. Gao, B. Tian, G. Y. & Si, D. "Physic perspective fusion of electromagnetic acoustic transducer and pulsed eddy current testing in non-destructive testing system." Philosophical Transactions of The Royal Society A Mathematical Physical and Engineering Sciences 378.2182(2020):20190608.

[20] Bang, Su Sik, Yeong Ho Lee, and Yong-June Shin. "Defect Detection in Pipelines via Guided Wave-Based Time–Frequency-Domain Reflectometry." IEEE Transactions on Instrumentation and Measurement 70 (2021): 1-11.

[21] H. Li, B. Gao, L. Miao, D. Liu, and W. L. Woo, "Multiphysics Structured Eddy Current and Thermography Defects Diagnostics System in Moving Mode," IEEE Transactions on Industrial Informatics, vol. PP, no. 99, pp. 1-1, 2020.

[22] N. Zhang, C. Ye, L. Peng, and Y. Tao, "Eddy Current Probe with Three-Phase Excitation and Integrated Array TMR Sensors," IEEE Transactions on Industrial Electronics, vol. PP, no. 99, pp. 1-1, 2020.

[23] Y. Gotoh and N. Takahashi, "Three-dimensional FEM analysis of electromagnetic inspection of outer side defects on steel tube using inner coil," IEEE transactions on magnetics, vol. 43, no. 4, pp. 1733-1736, 2007.

[24] M. Toharaand and Y. Gotoh, "Inspection Method of Outer Side Defect in Ferromagnetic Steel Tube by Insertion-Type Electromagnetic Sensor Using Square Wave Alternating Magnetic Field With DC Bias," in IEEE Transactions on Magnetics, vol. 57, no. 2, pp. 1-5, Feb. 2021.

[25] B., Liu, Y., Cao, H., & Zhang, et al. "Weak magnetic flux leakage: A possible method for studying pipeline defects located either inside or outside the structures." Ndt & E International (2015).

[26] Y. Gao, G. Y. Tian, K. Li, J. Ji, P. Wang, and H. Wang, "Multiple cracks detection and visualization using magnetic flux leakage and eddy current pulsed thermography," Sensors & Actuators A Physical, 2015.

[27] Daryabor, P. and M. S. Saflzadeh . "Image Fusion of Ultrasonic and Thermographic Inspection of Carbon/Epoxy Patches Bonded to an Aluminum Plate." Ndt & E International 90.sep.(2017):1-10.

[28] Chen, Kefan, et al. "Differential coupling double-layer coil for eddy current testing with high lift-off." IEEE Sensors Journal 21.16 (2021): 18146-18155.

[29] Sun, Y. and Y. Kang . "The feasibility of MFL inspection for omni-directional defects under a unidirectional magnetization." International Journal of Applied Electromagnetics and Mechanics 33.3-4(2010):919-925.

[30] Xiao Q, Feng J, Xu Z, et al. Receiver Signal Analysis on Geometry and Excitation Parameters of Remote Field Eddy Current Probe[J]. IEEE Transactions on Industrial Electronics, 2021, 99(1):1-10.

[31] Pham, H. Q. , Tran, B. V. , Doan, D. T. , Le, V. S. , Pham, Q. N. , & Kim, K. , et al., "Highly Sensitive Planar Hall Magnetoresistive Sensor for Magnetic Flux Leakage Pipeline Inspection," IEEE Transactions on Magnetics, pp. 1-5, 2018.

[32] M. M. Tehranchi, M. Ranjbaran, and H. Eftekhari, "Double core giant magneto-impedance sensors for the inspection of magnetic flux leakage from metal surface cracks," Sensors & Actuators A Physical, vol. 170, no. 1-2, pp. 55-61, 2011.

[33] Deif S, Daneshmand M. Multiresonant Chipless RFID Array System for Coating Defect Detection and Corrosion Prediction[J]. IEEE Transactions on Industrial Electronics, 2020, 67(10):8868-8877.

[34] Piao, G. Guo, J. , Hu, T. , Leung, H. , & Y Deng., et al. "Fast reconstruction of 3-D defect profile from MFL signals using key physics-based parameters and SVM." NDT & E International 103.APR.(2019):26-38.

[35] Z. Liu, B. Gao, and G. Y. Tian, "Natural Crack Diagnosis System Based on Novel L-Shaped Electromagnetic Sensing Thermography," IEEE Transactions on Industrial Electronics, vol. 67, no. 11, pp. 9703-9714, 2020.

[36] Zhu, Z. Q. Pang, Y. Howe, D. , Iwasaki, S. , Deodhar, R. , & Pride, A. "Analysis of electromagnetic performance of flux-switching permanent-magnet Machines by nonlinear adaptive lumped parameter magnetic circuit model." IEEE Transactions on Magnetics 41.11(2005):4277-4287.

[37] X Yuan, Li, W. Chen, G. X Yin, Jiang, W. & J Zhao, et al., "Inspection of both inner and outer cracks in aluminum tubes using double frequency circumferential current field testing method," Mechanical Systems and Signal Processing, vol. 127, no. JUL.15, pp. 16-34, 2019.

[38] Z. Deng, Y. Sun, Y. Kang, S. Kai, and R. Wang, "A Permeability-Measuring Magnetic Flux Leakage Method for Inner Surface Crack in Thick-Walled Steel Pipe," Journal of Nondestructive Evaluation, vol. 36, no. 4, p. 68, 2017.

Gaige Ru received the M.Sc. degree in control science and engineering from the Anhui Polytechnic University Wuhu, China, in 2019. He is currently pursuing the Ph.D. degree with the University of Electronic Science and Technology of China, Chengdu, China. His research mainly focuses on eddy current testing and magnetic flux leakage testing and instrumentation manufacturing. His research interests include smart sensors and system design for pipeline inspection.

Bin Gao (M' 12-SM' 14) received his B.Sc. degree in communications and signal processing from Southwest Jiao Tong University (2001-2005), China, MSc degree in communications and signal processing with Distinction and PhD degree from Newcastle University, UK (2006-2011). He worked as a Research Associate (2011-2013) with the same university on wearable acoustic sensor technology. Currently, he is a Professor with the School of Automation Engineering, University of Electronic Science and Technology of China (UESTC), Chengdu, China. His research interests include electromagnetic and thermography sensing, machine learning, nondestructive testing and evaluation where he actively publishes in these areas. He is also a very active reviewer for many international journals and long standing conferences. He has coordinated several research projects from National Natural Science Foundation of China. Personal web: http://faculty.uestc.edu.cn/gaobin/zh_CN/lwcg/153392/list/index.htm

Dong Liu graduated from college of physics, Sichuan University, Chengdu, China, in 2004. He received the M.Sc. degree and Ph.D. degree in control science and Engineering, University of Electronic Science and Technology, Chengdu, China, in 2010 and 2017, respectively. He is currently a post-doctoral student with the School of Automation Engineering, University of Electronic Science and Technology of China, Chengdu, China. His research interests include crystal oscillators, piezoelectric sensor, humidity sensors and eddy current sensor.

Qiuping Ma received the B.Sc. degree in Electronic Information Engineering from Sichuan Normal University (2013-2017), Chengdu, China. She is currently pursuing the Ph.D. degree in Electromagnetic Nondestructive Evaluation at the University of Electronic Science and Technology of China, Chengdu, China. Her research interests include smart sensors and system design for pipeline inspection.

School of Automation Engineering, University of Electronic Science and Technology of China, Chengdu, China

Haoran Li received the B.Sc. degree in electrical engineering and automation and the M.Sc. degree in control science and engineering from the Southwest University of Science and Technology, Mianyang, China, in 2015 and 2018, respectively. He is currently pursuing the Ph.D. degree with the University of Electronic Science and Technology of China, Chengdu, China. His research mainly focuses on eddy current testing and thermography and instrumentation manufacturing.

Wai Lok Woo (M'11–SM'12) received the B.Eng. degree in electrical and electronics engineering, and the M.Sc. and Ph.D. degrees in statistical machine learning from Newcastle University, U.K., in 1993, 1995, and 1998, respectively. He was the Director of research for the Newcastle Research and Innovation Institute, and the Director of operations for Newcastle University. He is currently a Professor of Machine Learning with Northumbria University, U.K. He has published more than 400 papers on these topics on various journals and international conference proceedings. His research interests include the mathematical theory and algorithms for data science and analytics, artificial intelligence, machine learning, data mining, latent component analysis, multidimensional signal, and image processing. He is a Member of the Institution Engineering Technology. He was a recipient of the IEE Prize and the British Commonwealth Scholarship. He serves as an Associate Editor to several international signal processing journals, including IET Signal Processing, the Journal of Computers, and the Journal of Electrical and Computer Engineering